Available online at www.sciencedirect.com
SCIENCE DIRECT®
Journal of Sound and Vibration 264 (2003) 639–655
JOURNAL OF SOUND AND VIBRATION
www.elsevier.com/locate/jsvi

Matching of asymptotic models in scattering of a plane acoustic wave by an elastic cylindrical shell

J.D. Kaplunov[a,*], V.A. Kovalev[b], M.V. Wilde[c]

[a] *Department of Mathematics, The University of Manchester, Oxford Road, Manchester M13 9PL, UK*
[b] *Department of Mathematics, Moscow State Academy of Device-Building and Computer Science, Ul. Stromynka 20, GSP-6, Moscow 107846, Russia*
[c] *Department of Mathematical Elasticity and Biomechanics, Saratov State University, Astrakhanskaya str. 83, Saratov 410026, Russia*

Received 29 October 2001; accepted 26 June 2002

Abstract

Scattering of a plane harmonic acoustic wave by an elastic cylindrical shell is considered. The procedure based on matching of asymptotic models is developed. The long-wave models (the Kirchhoff–Love theory (or its refinement) and the long-wave high-frequency approximation) are exploited in the vicinities of zero frequency and thickness resonance frequencies, whilst the model of a fluid-loaded flat elastic layer is utilized outside the aforementioned vicinities. Comparison with the exact solution demonstrates that the proposed approach is highly efficient for total synthesis of the scattered pressure as well as for uniform approximation of the resonant curves associated with partial modes.

1. Introduction

A modern version of the dynamic shell theory is based on matched asymptotic approximations of 3-D elasticity (e.g., see, Ref. [1]). Apart from the classical Kirchhoff–Love theory, which may be, to some extent, treated as the leading low-frequency approximation, there also exist two types of high-frequency approximations. In the case of the high-frequency short-wave approximation the effect of curvature becomes, as a rule, secondary. For example, the short-wave vibrations of a cylindrical shell can be analyzed starting from the model of a flat layer. The high-frequency long-wave approximation corresponds to the 2-D theory of thickness vibrations describing slowly varying motions in the vicinities of thickness stretch and shear resonance frequencies.

*Corresponding author. Tel.: +44-161-275-5800; fax: +44-161-275-5819.
E-mail address: kaplunov@ma.man.ac.uk (J.D. Kaplunov).

0022-460X/03/$ - see front matter
PII: S0022-460X(02)01212-9

It is of particular importance that the ranges of applicability for the long-wave approximations overlap that for the short-wave one. The relevant overlap regions lie near zero frequency and the thickness resonance frequencies. The simplest numerical illustration for matching of the aforementioned asymptotic models is presented in Ref. [2] (results of this paper are included in the monograph [1]) dealing with the total synthesis of the dispersion curves for a cylindrical shell starting from the Kirchhoff–Love theory, the theory of thickness (high-frequency long-wave) vibrations and plane (anti-plane) elasticity.

The consideration below represents, in a sense, an extension of the procedure described in Ref. [2] to problems of fluid–structure interaction. In the latter case all the asymptotic models have to be adapted to the contact conditions simulating fluid loading. In particular, the traditional low-frequency model of fluid–structure interaction based on the Kirchhoff–Love theory may be considerably improved by taking into account the normal compression of a shell by a fluid along with some other refinements (for details see, Ref. [3]). In this paper we introduce the model of a fluid-loaded flat elastic layer for describing forced short-wave motions. Before the flat layer model was used only for computing resonance scattering frequencies on the basis of Rayleigh–Lamb-type dispersion equations (e.g., see Ref. [4]). Neither resonance curves nor form functions were evaluated. We do not express in the equations of shell motion the scattered pressure in terms of slowly varying displacement amplitudes when dealing with the high-frequency long-wave model. A slightly different approach was developed in Ref. [5] (see also Ref. [1]).

In this paper the scheme making use of matching asymptotic models is applied to scattering of a plane harmonic acoustic wave by a thin cylindrical shell. Efficiency of the proposed methodology is demonstrated by comparison with the exact solution based on plane elasticity for describing shell motion. Both the form function and the resonant curves for partial modes are analyzed. Existence of overlap regions for the ranges of applicability in the case of various models is thoroughly investigated.

The paper is organized as follows. The original scattering problem is specified in Section 2. In particular, the series in Bessel functions are written out for the pressure in the incident and scattered waves. The utilized asymptotic models are introduced in Sections 3–5. All the basic relations are accompanied by necessary explanations. The relevant analytic solutions are obtained for the scattered pressure. In addition, the exact solution, corresponding to plane elasticity for cylindrical co-ordinates, is presented in the appendix. Section 6 is the key one for the paper. It represents a numerical illustration of the developed matching procedure.

2. Statement of the problem

Let the plane acoustic wave

$$p_i = p_0 \exp[-\mathrm{i}(k\xi + \omega t)] \tag{2.1}$$

be scattered by a circular cylindrical shell.

In the formula above p_i is the pressure in the incident wave, p_0 is a constant, ω is the circular frequency, k is the wave number, t is the time, ξ and is the distance from the shell axis.

Now introduce the dimensionless parameters

$$\kappa = \frac{\rho}{\rho_1}, \quad \beta_i = \frac{c_i}{c} \quad (i = 1, 2), \quad \vartheta = \frac{c_2}{c_1}, \quad k = \frac{\omega}{c}, \tag{2.2}$$

where c_1 and c_2 are the dilatation and distortion wave speeds in the material of the shell, ρ_1 is the mass density of the shell, c is the sound speed in the fluid, and ρ is the mass density of the fluid. The shell half-thickness h and the radius of the mid-surface R can be expressed in terms of its inner and outer radii a and b as $h = (a - b)/2$ and $R = (a + b)/2$.

In cylindrical co-ordinates r, θ ($\xi = r\cos\theta$) the pressure in the incident wave becomes [6]

$$p_i = p_0 \exp(-\mathrm{i}\omega t) \sum_{n=0}^{\infty} E_n (-\mathrm{i})^n \, \mathrm{J}_n(kr) \cos n\theta \tag{2.3}$$

with

$$E_0 = 1, \quad E_n = 2 \quad (n \geqslant 1),$$

where J_n is a cylindrical Bessel function of the first kind.

The scattered pressure can be written as

$$p_s = p_0 \exp(-\mathrm{i}\omega t) \sum_{n=0}^{\infty} E_n (-\mathrm{i})^n B_n \mathrm{H}_n^{(1)}(kr) \cos n\theta, \tag{2.4}$$

where $\mathrm{H}_n^{(1)}$ is a Hankel function of the first kind. It is clear that representations (2.3) and (2.4) satisfy the Helmholz equation describing fluid motion. In addition, the scattered pressure p_s obeys the radiation condition at infinity. The coefficients B_n have to be defined by solving the contact problem for the equations of shell motion. The solution corresponding to plane elasticity is presented in the appendix.

Below a start is made from asymptotic models of fluid–structure interaction oriented to thin shells. For the latter

$$\eta = \frac{h}{R} \to 0. \tag{2.5}$$

3. Fluid-loaded flat elastic layer

The flat layer model is based on an analogy between the peripheral waves arising in thin shells when scattering acoustic waves and the well-known Lamb waves propagating in flat elastic layers. Its range of applicability is restricted only to short-wave shell motions that are not strongly affected by the shell curvature. Therefore, the model is not valid in the vicinities of zero frequency and thickness resonance frequencies in which long peripheral waves occur. The model of a "dry" flat elastic layer previously was intensively used only for estimation of resonance frequencies (see, e.g., Ref. [4]). The related procedure involves substituting of a co-sinusoidal law for the nth mode (see series (2.3) and (2.4)) into the equations of plane elasticity for a flat layer with traction free faces, specified in Cartesian co-ordinates. In this case the number n corresponds to the wave number of Lamb waves. The developed model of a fluid-loaded flat elastic layer represents a natural generalization of the dry layer model incorporating the contact with environment along

the outer shell face; in doing so, it allows calculating of the scattered pressure as well as the resonant curves for partial modes.

In Cartesian co-ordinates θ, ζ ($\zeta = r/R - 1$), the equations of short-wave shell motion become

$$\Delta_p\varphi + \beta_1^{-2}k^2R^2\varphi = 0, \quad \Delta_p\psi + \beta_2^{-2}k^2R^2\psi = 0 \tag{3.1}$$

with

$$\Delta_p = \frac{\partial^2}{\partial\zeta^2} + \frac{\partial^2}{\partial\theta^2}, \tag{3.2}$$

where φ and ψ are the Lame potentials. The displacements and stresses are expressed as follows:

$$u_r = \frac{1}{R}\left(\frac{\partial\varphi}{\partial\zeta} + \frac{\partial\psi}{\partial\theta}\right), \quad u_\theta = \frac{1}{R}\left(\frac{\partial\varphi}{\partial\theta} - \frac{\partial\psi}{\partial\zeta}\right) \tag{3.3}$$

and

$$\sigma_r = \rho_1 c^2 \frac{1}{R^2}\left[-k^2R^2\varphi + 2\beta_2^2\left(\frac{\partial^2\psi}{\partial\zeta\partial\theta} - \frac{\partial^2\varphi}{\partial\theta^2}\right)\right],$$
$$\sigma_{r\theta} = \rho_1 c^2 \frac{1}{R^2}\left[k^2R^2\psi + 2\beta_2^2\left(\frac{\partial^2\varphi}{\partial\zeta\,\partial\theta} + \frac{\partial^2\psi}{\partial\theta^2}\right)\right]. \tag{3.4}$$

Eqs. (3.1)–(3.4) are valid provided that

$$\frac{\partial}{\partial\theta} \sim \frac{\omega R}{c_2} \gg 1, \tag{3.5}$$

i.e., for short-wave motions associated with large number of partial modes ($n \gg 1$). In this case the original equations of motion written in curvilinear (cylindrical) co-ordinates allow, in the leading order, replacing them by Cartesian co-ordinates; in doing so, one keeps only highest derivatives and fix the radial co-ordinate on the mid-surface of the shell.

All the other relations of the scattering problem considered do not change. In particular, the boundary conditions on shell faces can be written as

$$\sigma_r|_{\zeta=\eta} = -(p_i + p_s)|_{r=a}, \quad u_r|_{\zeta=\eta} = \frac{1}{\rho c^2 k^2}\frac{\partial}{\partial r}(p_i + p_s)\Big|_{r=a},$$
$$\sigma_{r\theta}|_{\zeta=\eta} = 0, \quad \sigma_r|_{\zeta=-\eta} = 0, \quad \sigma_{r\theta}|_{\zeta=-\eta} = 0 \tag{3.6}$$

with p_i and p_s defined by Eqs. (2.3) and (2.4), respectively.

By solving the formulated problem we determine the sought-for coefficients B_n. They are

$$B_n = -\frac{\mathrm{J}_n'(x)d_1 - 2k^3R^3\kappa\mathrm{J}_n(x)d_2}{\mathrm{H}_n^{(1)'}(x)d_1 - 2k^3R^3\kappa\mathrm{H}_n^{(1)}(x)d_2}, \tag{3.7}$$

where

$$d_1 = 4D_sD_a, \quad d_2 = \alpha_1(\sinh(\alpha_1\eta)\sinh(\alpha_2\eta)D_a + \cosh(\alpha_1\eta)\cosh(\alpha_2\eta)D_s),$$
$$x = ka$$

and where

$$D_s = \gamma^4 \cosh(\alpha_1\eta)\sinh(\alpha_2\eta) - 4\beta_2^4 n^2 \alpha_1\alpha_2 \sinh(\alpha_1\eta)\cosh(\alpha_2\eta),$$
$$D_a = \gamma^4 \sinh(\alpha_1\eta)\cosh(\alpha_2\eta) - 4\beta_2^4 n^2 \alpha_1\alpha_2 \cosh(\alpha_1\eta)\sinh(\alpha_2\eta)$$

with

$$\gamma^2 = 2n^2\beta_2^2 - k^2R^2, \quad \alpha_i = \sqrt{n^2 - \beta_i^{-2}k^2R^2} \quad (i = 1, 2).$$

4. Kirchhoff–Love theory of shells and its refinement

The classical Kirchhoff–Love theory as well as its refinement may be treated as low-frequency asymptotic expansions of the dynamic equations in elasticity. Therefore, these theories are adequate only near zero frequency. In this paper, we utilize the refined Kirchhoff–Love theory adapted for the problems in fluid–structure interaction in Ref. [3] (also see Ref. [1]). In addition to the classical formulation, it takes into account the normal compression of a shell by a fluid and more sophisticated distributions along the shell thickness and allows better approximations for "exact" dispersion curves.

The equations of motion in the aforementioned refined theory are

$$\left(1 + \frac{1}{3}\eta^2\right)\frac{\partial^2 v}{\partial\theta^2} + \frac{\partial w}{\partial\theta} - \frac{1}{3}\eta^2\frac{\partial^3 w}{\partial\theta^3} + \frac{1-\nu}{2}R^2\frac{\omega_{tg}^2}{c_2^2}v + \underline{\frac{\nu(1+\nu)R}{2E}\frac{\partial m}{\partial\theta}} = 0, \tag{4.1}$$

$$\frac{\partial v}{\partial\theta} - \frac{1}{3}\eta^2\frac{\partial^3 v}{\partial\theta^3} + w + \frac{1}{3}\eta^2\frac{\partial^4 w}{\partial\theta^4} - \frac{1-\nu}{2}R^2\frac{\omega_{tr}^2}{c_2^2}w + \underline{\frac{\nu(1+\nu)R}{E}m} + \frac{(1-\nu^2)R^2}{2Eh}Z = 0,$$

where

$$Z = \left(1 - \underline{\frac{8-3\nu}{10(1-\nu)}\eta^2\frac{\partial^2}{\partial\theta^2}}\right)(p_i + p_s)\Big|_{r=a}, \quad m = -(p_i + p_s)|_{r=a}, \tag{4.2}$$

$$\omega_{tg}^2 v = \omega^2\left[v + \underline{\eta^2(b_0 + b_1z^2 + b_2z^4)\frac{\partial^2 v}{\partial\theta^2}}\right], \tag{4.3}$$

$$\omega_{tr}^2 w = \omega^2\left[1 + \underline{a_1z + a_2z^2 + a_3z^3}\right]w \tag{4.4}$$

with

$$b_0 = -\frac{\nu^2}{3(1-\nu)^2}, \quad b_1 = -\frac{\nu^2(3 - 5\nu - \nu^2)}{45(1-\nu)^3},$$
$$b_2 = \frac{\nu^2(-17 + 56\nu - 33\nu^2 - 28\nu^3 + 5\nu^4)}{1260(1-\nu)^4}, \tag{4.5}$$

$$a_1 = \sqrt{\frac{3}{2}(1-\nu)}\frac{17-7\nu}{15(1-\nu)}, \quad a_2 = \frac{1179-818\nu+409\nu^2}{2100(1-\nu)},$$
$$a_3 = \sqrt{\frac{3}{2}(1-\nu)}\frac{5951-2603\nu+9953\nu^2-4901\nu^3}{126\,000(1-\nu)^2} \tag{4.6}$$

and

$$z = \frac{\omega h}{c_2}. \tag{4.7}$$

Here v is the tangential displacement of the mid-surface along the axis θ, w is the transverse displacement of the mid-surface, E is Young's modulus, and ν is the Poisson ratio.

The impenetrability condition for the refined theory is

$$w + \underline{\frac{\nu\eta^2}{2(1-\nu)}\frac{\partial^2 w}{\partial\theta^2} - \frac{\nu\eta}{(1-\nu)}\frac{\partial v}{\partial\theta}} = \frac{1}{\rho\omega^2}\frac{\partial}{\partial r}(p_i + p_s)\bigg|_{r=a}. \tag{4.8}$$

The underlined terms in equations above take into account the normal compression of a shell by a fluid in Eq. (4.1), improved approximations for dispersion curves in Eqs. (4.3) and (4.4), correction for fluid loading in Eq. (4.2) and deviation of the mid-surface deflection w from that on the outer surface $r = a$ in the impenetrability condition (4.8). By neglecting all of them one arrives at the model corresponding to the classical Kirchhoff–Love theory. The quantities p_i and p_s in the formulae above are given by Eqs. (2.3) and (2.4) as before.

In the case under consideration the coefficients B_n become

$$B_n = -\frac{d_1 \mathrm{J}_n'(x) + \frac{1}{4}\kappa R\beta_2^{-2}(e_2 d_2 + e_1 d_3)k\mathrm{J}_n(x)}{d_1 \mathrm{H}_n^{(1)'}(x) + \frac{1}{4}\kappa R\beta_2^{-2}(e_2 d_2 + e_1 d_3)k\mathrm{H}_n^{(1)}(x)}, \tag{4.9}$$

where

$$d_1 = \begin{vmatrix} a_{11} & a_{12} \\ a_{21} & a_{22} \end{vmatrix}, \quad d_2 = \begin{vmatrix} a_{12} & a_{11} \\ a_{32} & a_{31} \end{vmatrix}, \quad d_3 = \begin{vmatrix} a_{21} & a_{22} \\ a_{31} & a_{32} \end{vmatrix}$$

with

$$a_{11} = -n^2\left(1 + \frac{1}{3}\eta^2\right) + \frac{1-\nu}{2}R^2\frac{\omega_{tg}^2}{c_2^2}, \quad a_{12} = -n\left(1 + \frac{1}{3}\eta^2 n^2\right), \tag{4.10}$$

$$a_{21} = -n\left(1 + \frac{1}{3}\eta^2 n^2\right), \quad a_{22} = 1 + \frac{1}{3}\eta^2 n^4 - \frac{1-\nu}{2}R^2\frac{\omega_{\mathrm{tr}}^2}{c_2^2},$$

$$a_{31} = -\frac{\nu}{1-\nu}\eta n, \quad a_{32} = 1 - \frac{\nu}{2(1-\nu)}\eta^2 n^2,$$
$$e_1 = -\nu n, \quad e_2 = \nu - \frac{1-\nu}{\eta}\left(1 + \frac{8-3\nu}{10(1-\nu)}\eta^2 n^2\right).$$

As it is mentioned in Ref. [3], the range of applicability for the refined model is given by

$$\frac{\omega R}{c_2} \ll \eta^{-1}. \tag{4.11}$$

Whilst that for the model based on the classical Kirchhoff–Love theory is only

$$\frac{\omega R}{c_2} \ll \eta^{-1/2}. \tag{4.12}$$

Thus, both of these theories describe only the zero order Lamb-type waves S_0 and A_0 (or the fluid-born wave A). The relevant mode numbers lie in the ranges $n \ll \eta^{-1}$ and $n \ll \eta^{-1/2}$ for the refined asymptotic model and the Kirchhoff–Love theory, respectively.

5. Long-wave high-frequency approximation

To describe first modes of higher order Lamb-type waves we start from the asymptotic theory for long-wave high-frequency vibrations of fluid-loaded shells. The latter represents, in the sense, a high-frequency analog of the classical Kirchhoff–Love theory dealing with slowly varying motions that arise in the vicinities of cut-offs located near thickness resonance frequencies of a flat layer with traction free faces. Similar to the classical shell theory the long-wave high-frequency model assumes reduction to lower dimensional equations by excluding the normal co-ordinate. In doing so, it operates with sinusoidal-type approximations along the shell thickness.

The theory in question (e.g., see, Refs. [1,5]) involves two types of asymptotic approximations. The transverse approximation (the transverse shell displacement dominates) is applicable in the vicinities of the thickness stretch resonance frequencies, i.e., at $|z - \Lambda_{st}| \ll 1$, where z is defined by formula (4.7) and $\Lambda_{st} = \pi m/\vartheta$ (for antisymmetric motions) or $\Lambda_{st} = \pi(2m-1)/2\vartheta$ (for symmetric motions); $m = 1, 2, \ldots$. The relevant one-dimensional equation is

$$\eta^2\left(T\frac{\partial^2 w_0}{\partial\theta^2} + T_R^0 w_0\right) + (z^2 - \Lambda_{st}^2)w_0 = \pm\frac{(-1)^m h}{\rho_1 c_2^2}(p_i + p_s)\left(1 + \frac{1}{2}\eta\right) \tag{5.1}$$

with

$$T_R^0 = \frac{1}{4\vartheta^2} - 4, \quad T = \frac{1}{\vartheta^2} \mp \frac{8}{\Lambda_{st}}\left\{\begin{array}{c}\tan\Lambda_{st}\\ \cot\Lambda_{st}\end{array}\right\}, \tag{5.2}$$

where $w_0(\theta)$ is the 1-D long-wave amplitude of the transverse displacement; here and further the upper (lower) sign and the upper (lower) expression in braces corresponds to antisymmetric (symmetric) modes.

The impenetrability condition can be written as

$$\pm(-1)^m w_0\left(1 - \frac{1}{2}\eta\right) = \frac{1}{\rho\omega^2}\frac{\partial}{\partial r}(p_i + p_s)\Big|_{r=a}. \tag{5.3}$$

In the vicinities of thickness shear resonance frequencies the tangential approximation (the tangential displacements exceed considerably the transverse one) is adequate. In this case the

governing equation becomes

$$\eta^2\left(P\frac{\partial^2 v_0}{\partial\theta^2}+P_R^0 v_0\right)+(z^2-\Lambda_{sh}^2)v_0=\frac{2(-1)^{m+1}h\vartheta\eta}{\Lambda_{sh}\rho_1 c_2^2}\frac{\partial(p_i+p_s)}{\partial\theta}\left\{\begin{array}{c}\cot(\vartheta\Lambda_{sh})\\ \tan(\vartheta\Lambda_{sh})\end{array}\right\} \tag{5.4}$$

with

$$P_R^0=-\frac{15}{4},\quad P=1\pm\frac{8\vartheta}{\Lambda_{st}}\left\{\begin{array}{c}\cot(\vartheta\Lambda_{sh})\\ \tan(\vartheta\Lambda_{sh})\end{array}\right\}, \tag{5.5}$$

where $v_0(\theta)$ is the 1-D long-wave amplitude of the tangential displacement.

Now the impenetrability condition reduces to

$$\frac{2(-1)^m\vartheta\eta}{\Lambda_{sh}}\frac{\partial v_0}{\partial\theta}\left\{\begin{array}{c}\cot(\vartheta\Lambda_{sh})\\ \tan(\vartheta\Lambda_{sh})\end{array}\right\}=\frac{1}{\rho\omega^2}\frac{\partial}{\partial r}(p_i+p_s)\Big|_{r=a}. \tag{5.6}$$

In Eqs. (5.4)–(5.6) $\Lambda_{sh}=\pi(2m-1)/2$ (for antisymmetric motions) and $\Lambda_{sh}=\pi m$ (for the symmetric motions); $m=1,2,\ldots$. They are valid at $|z-\Lambda_{sh}|\ll 1$.

Then representations (2.3) and (2.4) for the pressure p_i and p_s have to be introduced into Eqs. (5.1) and (5.4). By solving systems (5.1) and (5.3) or (5.4) and (5.6) the coefficients B_n are determined. In particular, for the antisymmetric tangential motions they are

$$B_n=-\frac{S\mathrm{J}_n'(x)-4n^2h\kappa\beta_1^{-2}(\cot^2(\vartheta\Lambda_{sh})/\Lambda_{sh}^2)k\mathrm{J}_n(x)}{S\mathrm{H}_n^{(1)'}(x)-4n^2h\kappa\beta_1^{-2}(\cot^2(\vartheta\Lambda_{sh})/\Lambda_{sh}^2)k\mathrm{H}_n^{(1)}(x)} \tag{5.7}$$

with

$$S=-Pn^2+P_R^0+\eta^{-2}(z^2-\Lambda_{sh}^2). \tag{5.8}$$

It is essential that solutions like Eq. (5.7) are applicable only for a few first modes ($n\ll\eta^{-1}$). At the same time, in the vicinities of thickness resonance frequencies we observe the resonances of higher angular modes ($n\sim\eta^{-1}$) associated, for example, with zero order Lamb-type waves. Therefore, for numerical computation of the scattered pressure the long-wave high-frequency approximation should be combined with the flat layer model.

6. Matching of asymptotic models

Consider matching of the asymptotic models involved. First, we study the resonance components of partial modes [4]. In the case of an acoustically rigid background they are expressed as

$$\zeta_n=\frac{4}{\sqrt{\pi x}}\left|B_n+\frac{\mathrm{J}_n'(x)}{\mathrm{H}_n^{(1)'}(x)}\right|. \tag{6.1}$$

The resonance components for the Lamb-type wave S_0 corresponding both to the refined Kirchhoff–Love theory and the flat layer model are plotted in Fig. 1. They are computed by formulae (6.1). The coefficients B_n are defined either by Eq. (4.9) (the refined Kirchhoff–Love theory) or by Eq. (3.7) (the flat layer model). The exact solution corresponding to plane elasticity

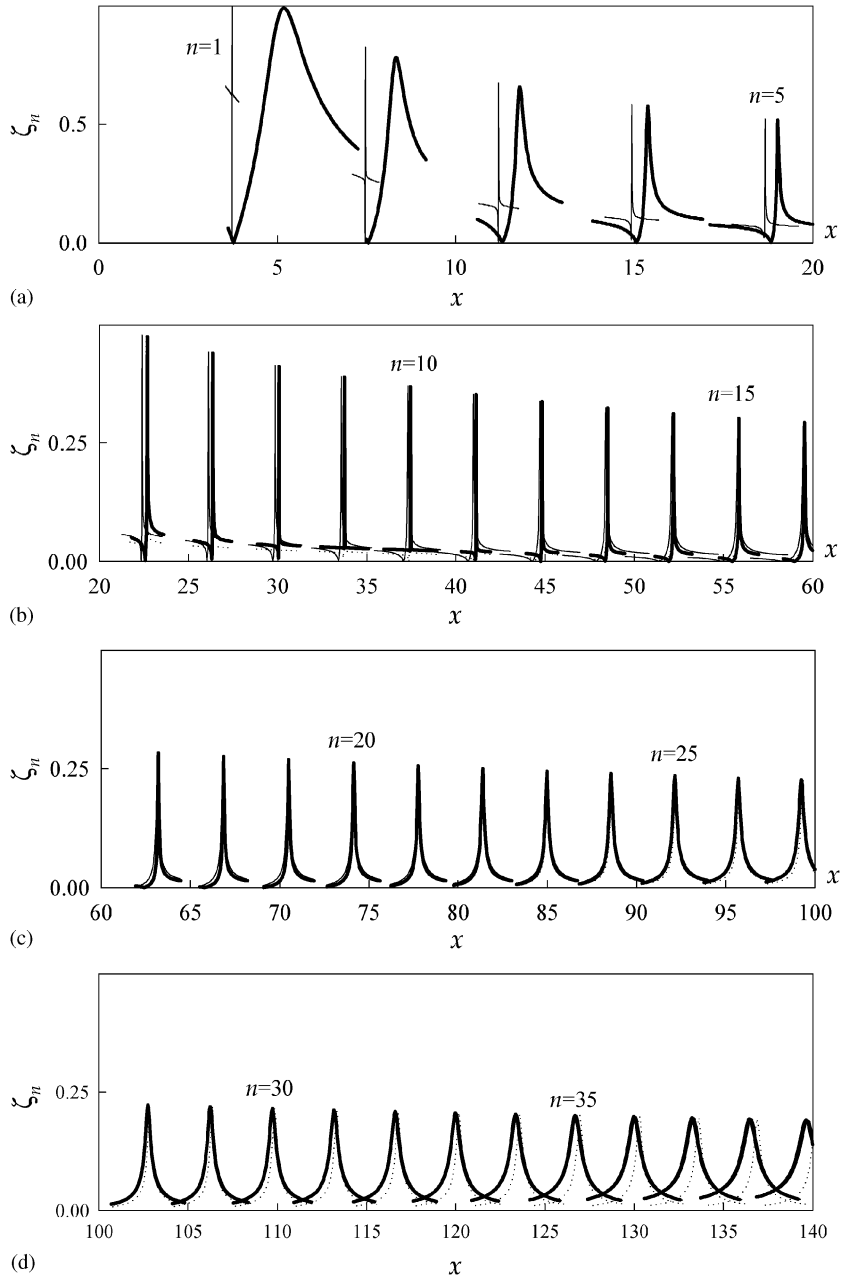

Fig. 1. The resonance components of the partial modes for the S_0 wave. The thick solid line corresponds to the exact solution, the dotted line to the refined Kirchhoff–Love theory and the thin solid line to the flat layer model.

(see the appendix) is also shown in this figure. The problem parameters are

$$c_1 = 5960\,\mathrm{m/s}, \quad c_2 = 3240\,\mathrm{m/s}, \quad c = 1493\,\mathrm{m/c},$$
$$\rho = 1000\,\mathrm{kg/m^3}, \quad \rho_1 = 7700\,\mathrm{kg/m^3}, \quad \eta = \tfrac{1}{39}. \tag{6.2}$$

The observation of Fig. 1 shows that both models possess a high accuracy over the region $30 \lesssim n \lesssim 100$. For small number modes ($n \lesssim 30$) the refined Kirchhoff–Love theory provides a better approximation, whereas for large number ones ($n \gtrsim 100$) the flat layer model appears to be more appropriate. Thus the ranges of applicability of two simplified numerical schemes overlap.

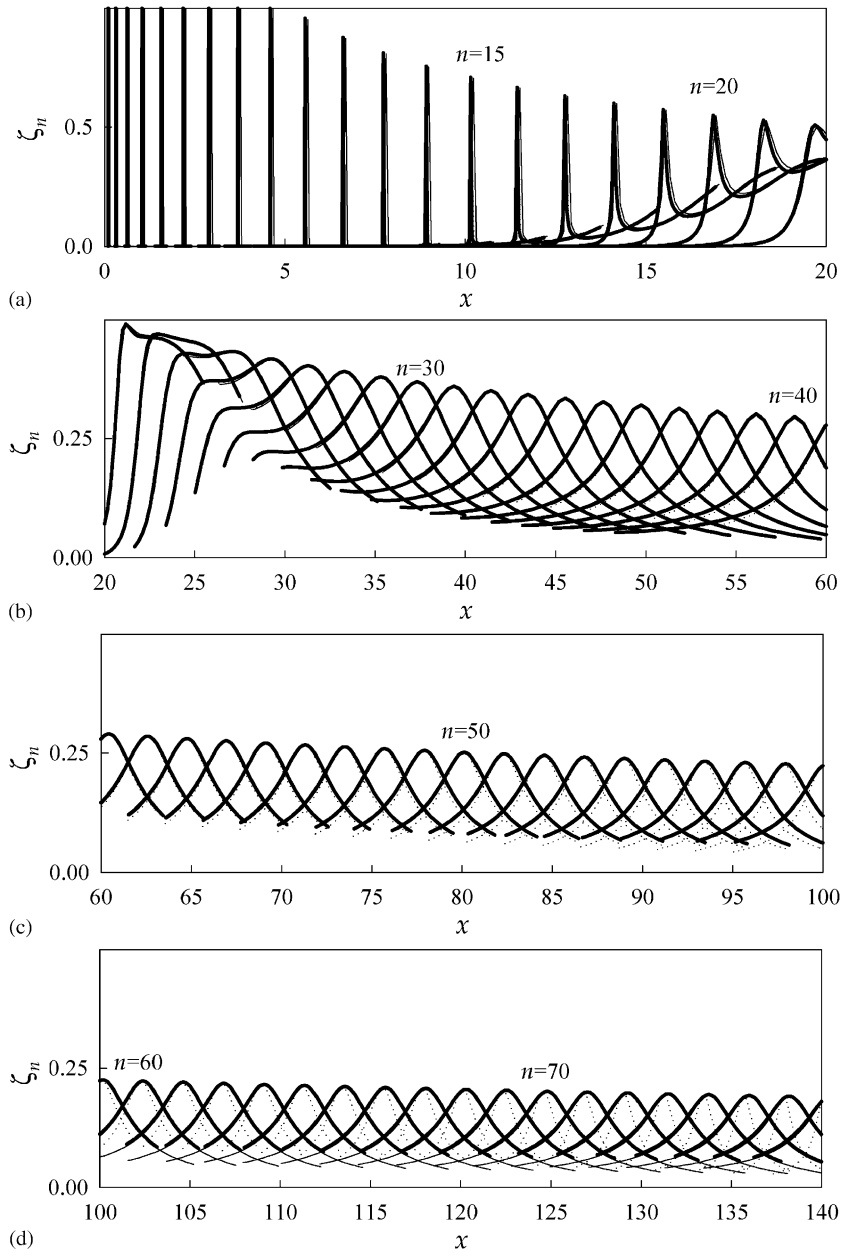

Fig. 2. The resonance components of the partial modes for the A and A_0 waves. Keys are as in Fig. 1.

An analogous comparison is presented in Fig. 2 for the fluid-born wave A (beginning with $n = 25$ it transforms to the Lamb-type wave A_0). In this case the overlap region may be roughly estimated by the inequality $20 \lesssim n \lesssim 80$.

In Fig. 3 the resonance components for the Lamb-type wave A_1 corresponding to the exact solution are compared with those associated with the flat layer model and the long-wave high-frequency approximation. For the latter the coefficients B_n are defined by Eq. (5.7). Fig. 3 demonstrates matching of lower quality compared with that in Figs. 1 and 2.

The approximation errors for dispersion curves are given in Fig. 4. In the case of a dry cylindrical shell similar calculations were presented in Ref. [2]. As usual in resonance scattering theory (e.g., see, Ref. [4]) the discrete mode number n in Fig. 4 is associated with the wave number of peripheral waves. The deviation Δn is plotted where

$$\Delta n = |n^{app} - n^{ex}| \tag{6.3}$$

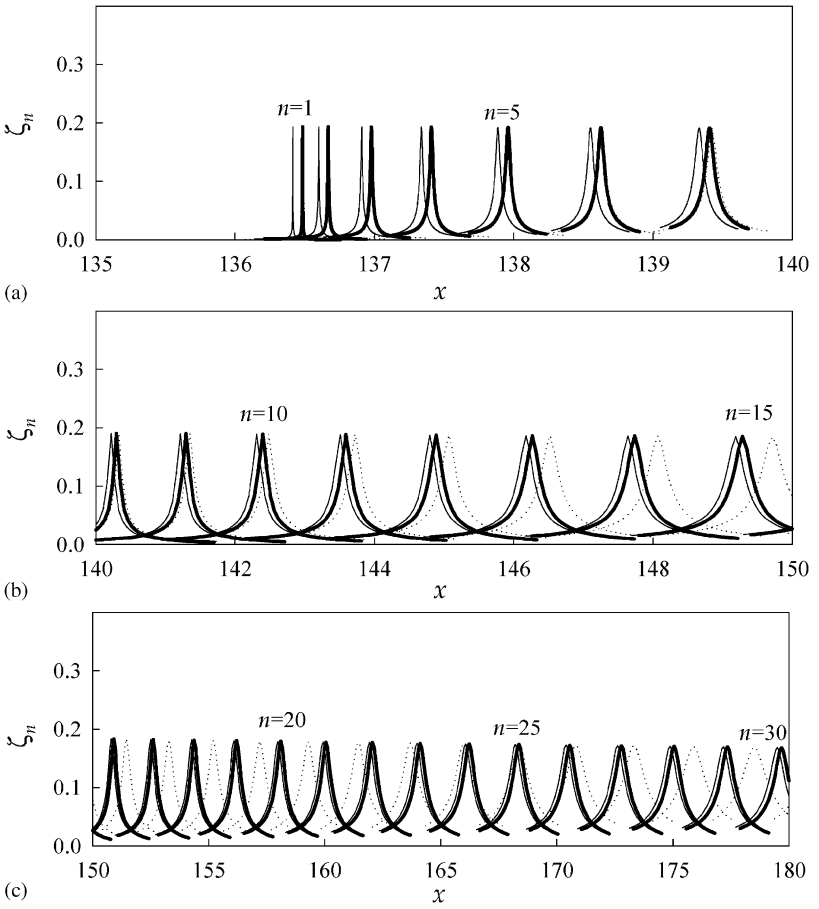

Fig. 3. The resonance components of the partial modes for the A_1 wave. The thick solid line corresponds to the exact solution, the dotted line to the long-wave high-frequency approximation and the thin solid line to the flat layer model.

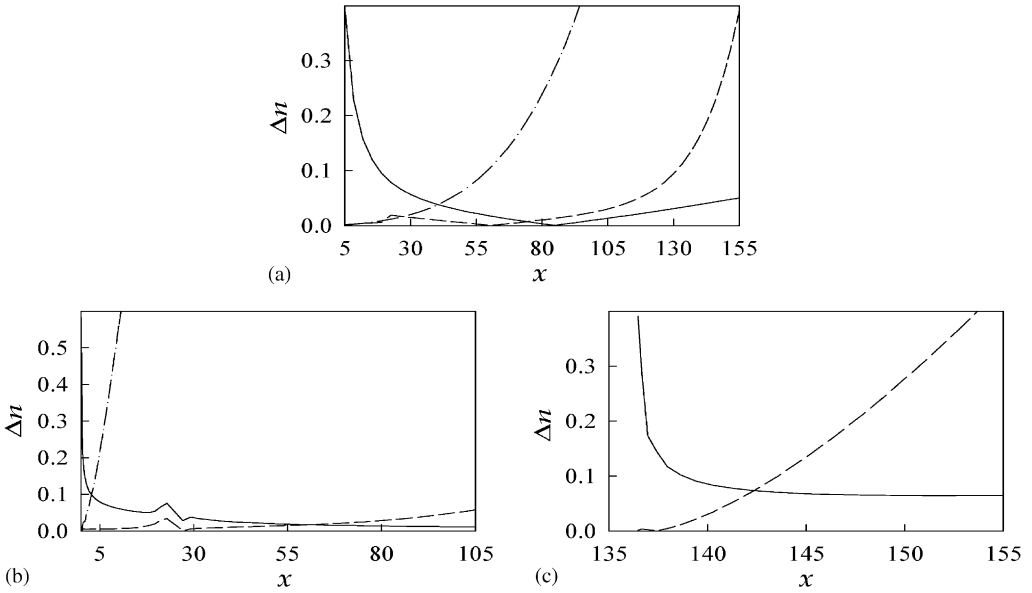

Fig. 4. The approximation error for the S_0 wave (a), for the A (A_0) wave (b), for the A_1 wave (c). The dashed line corresponds to the refined Kirchhoff–Love theory in (a) and (b) and to the long-wave high-frequency approximation in (c). The solid line corresponds to the flat layer model in all three figures and dotted–dashed line in (a) and (b) to the classical Kirchhoff–Love theory.

and n^{ex} is calculated on the basis of plane elasticity, n^{app} corresponds to various versions of the Kirchhoff–Love theory or the flat layer model (for Figs. 4a and b) and the long-wave high-frequency approximation or the flat layer model (for Fig. 4c).

Fig. 4 involves more specific numerical data related to overlap regions. These are located near the points where the curves meet corresponding to different asymptotic models. The flat layer model always provides better approximations above the frequencies corresponding to the aforementioned points while all the long-wave theories possess higher accuracy beyond them. The values Δn calculated at these points determine maximal approximation errors. The inequality $\Delta n < 1$ means that the error does not exceed the distance between neighboring resonance frequencies. Hence for a good approximation $\Delta n \ll 1$ is required.

The results related to synthesis of the form function for the far field ($r \to \infty$) in the case of backscattering ($\theta = 0$) are presented in Figs. 5 and 6. Starting from the formula

$$p = \frac{2}{\sqrt{\pi x}} \left| \sum_{n=0}^{\infty} E_n B_n (-1)^n \right|, \tag{6.4}$$

the long-wave high-frequency approximation is utilized beginning with the first thickness resonance frequency and only for $n < 10$. The rest of series (6.4) is evaluated by the flat layer model. The point is that the former does not describe large number resonance modes of the zero order waves S_0 and A_0(or A) occurring over this frequency domain. Location of the overlap regions in Figs. 5 and 6 agrees with observations above. The graphs in these figures confirm

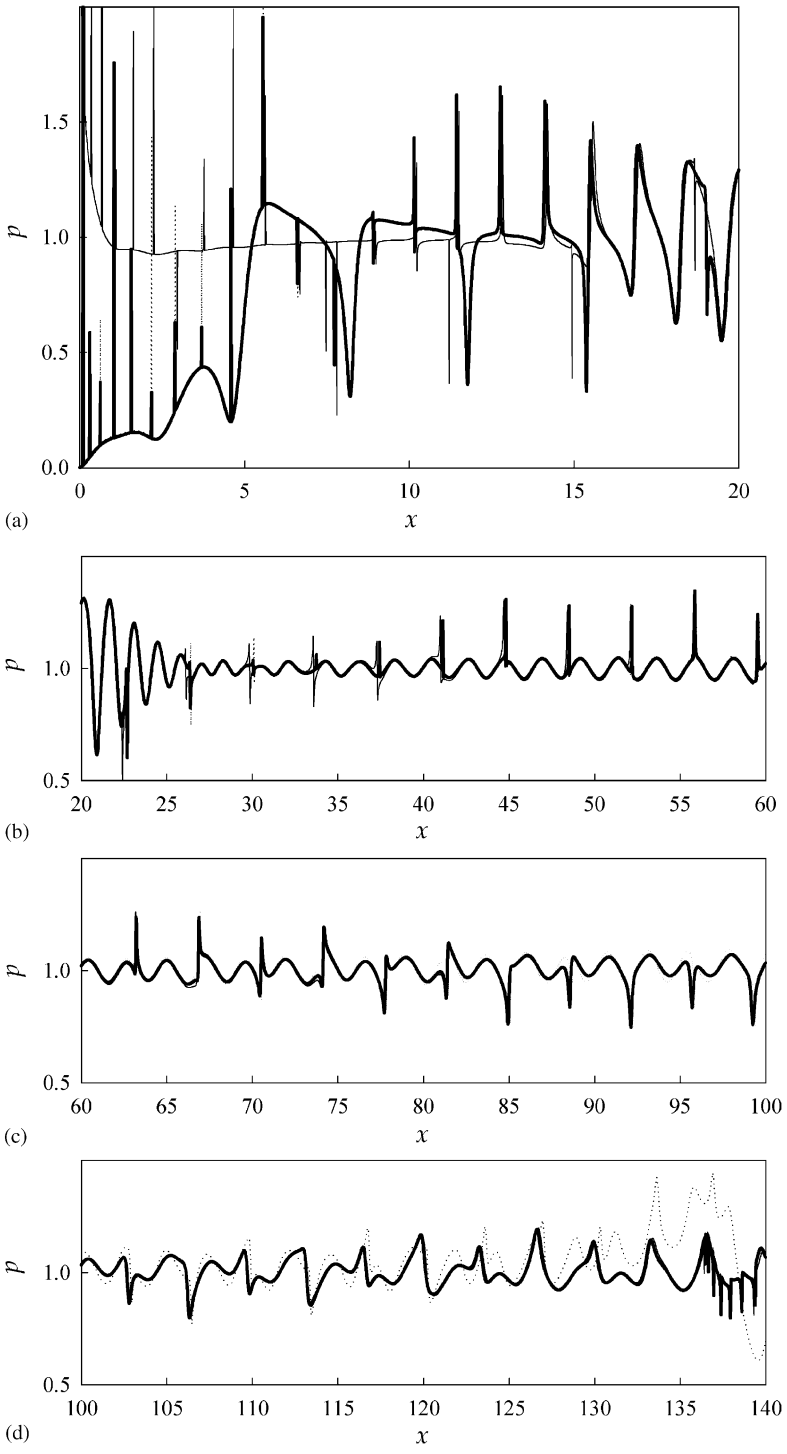

Fig. 5. Comparison of the form functions computed on the basis of the refined Kirchhoff–Love theory, the flat layer model and plane elasticity. Keys are as in Fig. 1.

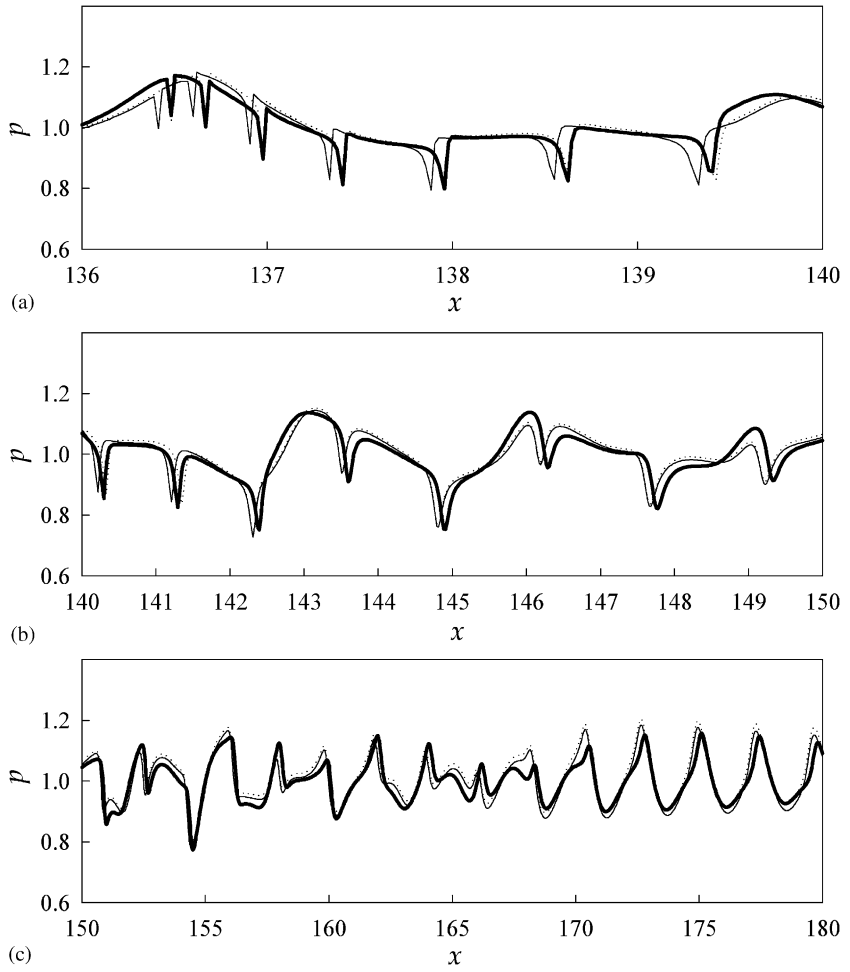

Fig. 6. Comparison of the form functions computed on the basis of the flat layer model, the long-wave high-frequency approximation and plane elasticity. Keys are as in Fig. 3.

efficiency of the proposed scheme consisting in utilizing three simpler matching models instead of the original one.

The form functions computed on the basis of the classical Kirchhoff–Love theory, the flat layer model and plane elasticity are plotted in Fig. 7. Comparison of the numerical data presented in Figs. 5 and 7 indicate a considerable advantage of the refined Kirchhoff–Love theory. However, for a thinner shell the classical Kirchhoff–Love theory may also be matched with the flat layer model since its accuracy increases, as the shell thickness tends to zero.

7. Concluding remarks

The numerical data presented demonstrate a high efficiency of the developed methodology. The latter may be easily generalized to scattering problems for shells of more complicated shape

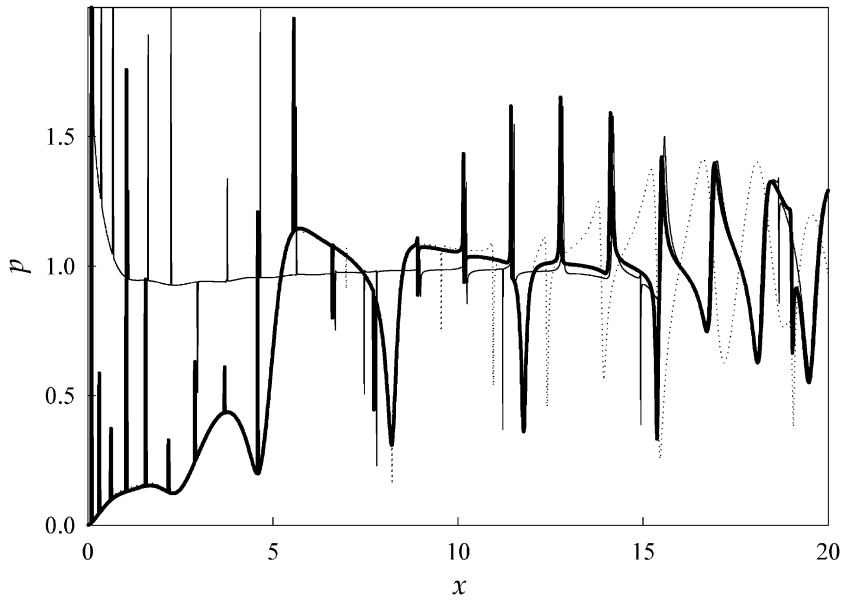

Fig. 7. Comparison of the form functions computed on the basis of the classical Kirchhoff–Love theory, the flat layer model and plane elasticity. The thick solid line corresponds to the exact solution, the dotted line to the Kirchhoff–Love theory and the thin solid line to the flat layer model.

subjected to arbitrary acoustic excitation. It is important to emphasize two peculiarities of the asymptotic models involved:

1. The refined version of the Kirchhoff–Love theory appears to be a better approximation in comparison with its classical analog. The former represents a model of the same complexity possessing a wider range of applicability.
2. The numerical procedures, utilized near thickness resonance frequencies, have to include both the long-wave high-frequency approximation and the model of a fluid-loaded flat elastic layer. The first is oriented to evaluate long-wave components (a few first terms in series (2.4)), while the second usually deals with short-wave components (all other terms in series (2.4)). The latter involve large number resonance modes associated, for example, with the zero order Lamb-type waves.

Acknowledgements

The research is partly supported by the Russian Foundation for Basic Research (Grant no. 02-01-00843) in the case of the first author and INTAS (Grant No. YSF 2001/1-7) in the case of the third author.

Appendix

In terms of plane elasticity shell motion is described by

$$\Delta\varphi + \beta_1^{-2}k^2R^2\varphi = 0, \quad \Delta\psi + \beta_2^{-2}k^2R^2\psi = 0, \tag{A.1}$$

where

$$\Delta = \frac{\partial^2}{\partial r^2} + \frac{1}{r}\frac{\partial}{\partial r} + \frac{1}{r^2}\frac{\partial^2}{\partial \theta^2} \tag{A.2}$$

and

$$u_r = \frac{\partial \varphi}{\partial r} + \frac{1}{r}\frac{\partial \psi}{\partial \theta}, \quad u_\theta = \frac{1}{r}\frac{\partial \varphi}{\partial \theta} - \frac{\partial \psi}{\partial r} \tag{A.3}$$

with

$$\begin{aligned} \sigma_r &= \rho_1 c^2 \left[-\left(\frac{\beta_1^2}{\beta_2^2} - 2\right) k^2 \varphi + 2\beta_2^2 \left(\frac{\partial^2 \varphi}{\partial r^2} + \frac{1}{r}\frac{\partial^2 \psi}{\partial \zeta\, \partial \theta} - \frac{1}{r^2}\frac{\partial \psi}{\partial \theta} \right) \right], \\ \sigma_{r\theta} &= \rho_1 c^2 \left[k^2 \psi + 2\beta_2^2 \left(\frac{1}{r}\frac{\partial^2 \varphi}{\partial \zeta\, \partial \theta} - \frac{1}{r^2}\frac{\partial \varphi}{\partial \theta} + \frac{1}{r^2}\frac{\partial^2 \psi}{\partial \theta^2} + \frac{1}{r}\frac{\partial \psi}{\partial r} \right) \right]. \end{aligned} \tag{A.4}$$

The boundary conditions are given by Eqs. (3.6). The coefficients B_n in formula (2.4) can be written as

$$B_n = \frac{L_n \mathrm{J}_n(x) - x\mathrm{J}_n'(x)}{L_n \mathrm{H}_n^{(1)}(x) - x\mathrm{H}_n^{(1)'}(x)} \tag{A.5}$$

with

$$L_n = \frac{\kappa D_n^{(1)}}{D_n^{(2)}}, \quad D_n^{(1)} = \begin{vmatrix} b_{11} & b_{12} & b_{13} & b_{14} \\ b_{31} & b_{32} & b_{33} & b_{34} \\ b_{41} & b_{42} & b_{43} & b_{44} \\ b_{51} & b_{52} & b_{53} & b_{54} \end{vmatrix}, \quad D_n^{(2)} = \begin{vmatrix} b_{21} & b_{22} & b_{23} & b_{24} \\ b_{31} & b_{32} & b_{33} & b_{34} \\ b_{41} & b_{42} & b_{43} & b_{44} \\ b_{51} & b_{52} & b_{53} & b_{54} \end{vmatrix}, \tag{A.6}$$

where

$$b_{11} = x_1 \mathrm{J}_n'(x_1), \quad b_{13} = n\mathrm{J}_n(x_2), \tag{A.7}$$

$$b_{21} = 2\frac{x_1^2}{x_2^2}\left[\left(\frac{1}{2}\frac{x_2^2}{x_1^2} - 1 \right) \mathrm{J}_n(x_1) - \mathrm{J}_n''(x_1) \right], \quad b_{23} = 2\frac{n}{x_2^2}\left[\mathrm{J}_n(x_2) - x_2 \mathrm{J}_n'(x_2) \right],$$

$$b_{31} = -2n\left[\mathrm{J}_n(x_1) - x_1 \mathrm{J}_n'(x_1) \right], \quad b_{33} = -2\left[(\tfrac{1}{2}x_2^2 - n^2)\mathrm{J}_n(x_2) + x_2 \mathrm{J}_n'(x_2) \right]$$

and where

$$x_i = \beta_i^{-1} x \quad (i = 1, 2). \tag{A.8}$$

The coefficients in the second and the fourth columns and in the third and the fourth rows of matrices (A.6) can be obtained from their analogs (A.7) by replacing the Bessel functions J_n by Y_n and the quantities x_i by

$$\tilde{x}_i = \frac{a - 2h}{a} x_i \quad (i = 1, 2). \tag{A.9}$$

References

[1] J.D. Kaplunov, L.Yu. Kossovich, E.V. Nolde, Dynamics of Thin Walled Elastic Bodies, Academic Press, San Diego, 1998.
[2] V.L. Beresin, L.Yu. Kossovich, J.D. Kaplunov, Synthesis of the dispersion curves for a cylindrical shell on the basis of approximate theories, Journal of Sound and Vibration 186 (1995) 37–53.
[3] A.V. Belov, J.D. Kaplunov, E.V. Nolde, A refined asymptotic model of fluid-structure interaction in scattering by elastic shells, Flow, Turbulence and Combustion 61 (1999) 255–267.
[4] N.D. Veksler, Resonance Acoustic Spectroscopy, Springer, Berlin, 1993.
[5] J.D. Kaplunov, High-frequency SSS of low variability in immersed shells, Prikladnaya Mathematica i Mekhanika (Journal of Applied Mathematics and Mechanics) 55 (1991) 478–485.
[6] P.M. Morse, H. Feshbach, Methods of Theoretical Physics, McGraw-Hill, New York, 1953.